IDENTIFICATION OF VEGETATED LANDSLIDES USING ONLY A LIDAR-BASED TERRAIN MODEL AND DERIVATIVES IN AN OBJECT-ORIENTED ENVIRONMENT

M. Van Den Eeckhaut [a, *], N. Kerle [b], J. Poesen [c], J. Hervás [a]

[a] Institute for Environment and Sustainability, Joint Research Centre (JRC), European Commission, 21027 Ispra, Italy - (miet.van-den-eeckhaut, javier.hervas)@jrc.ec.europa.eu
[b] Faculty of Geo-Information Science and Earth Observation, University of Twente, The Netherlands - Kerle@itc.nl
[c] Department Earth and Environmental Sciences, KU Leuven, Celestijnenlaan 200 E, B-3001 Heverlee, Belgium - jean.poesen@ees.kuleuven.be

KEY WORDS: Landslide identification, Dense vegetation, Conceptualisation, LiDAR, Segmentation, Classification, Geomorphometry, Belgium, Support vector machines

ABSTRACT:

Light Detection and Ranging (LiDAR) and its derivative products have become a powerful tool in landslide research, particularly for landslide identification and landslide inventory mapping. In contrast to the many studies that use expert-based analysis of LiDAR derivatives to identify landslides only few studies, all pixel-based, have attempted to develop computer-aided methods for extracting landslides from LiDAR. It has not been tested whether object-oriented analysis (OOA) could be an alternative. Therefore, this study investigates the application of OOA using 2 m resolution slope gradient, roughness, curvature, and openness maps calculated from single pulse LiDAR data, without the support of any spectral information. More specifically, the focus is on the possible use of these derivatives for segmentation and classification of slow-moving landslides in densely vegetated areas, where spectral data do not facilitate accurate landslide identification. A semi-quantitative method based on support vector machines (SVM) was developed for a test area in the Flemish Ardennes (Belgium). The procedure was then applied without further modification to a validation area in the same region. The results show that OOA using LiDAR derivatives allows recognition and characterization of profound morphologic properties of deep-seated landslides on soil-covered hillslopes such as those in the Flemish Ardennes, because approximately 70% of the landslides of an expert-based inventory were also included in the object-oriented inventory. For mountain areas with bedrock, on the other hand, it is expected more difficult to create a transferable model.

1. INTRODUCTION

Traditional methods of identifying landslides and analysing their geomorphometry involve expert-based mapping and measurement from topographic maps, aerial stereophotos, satellite imagery and digital elevation models (DEMs). Since the early 2000s, also Light Detection and Ranging (LiDAR) and its wide range of derivative products (e.g. shaded-relief, slope, surface roughness and contour maps) have become a popular and powerful tool, especially for landslide inventory mapping in forested areas (e.g. Schulz, 2004; Van Den Eeckhaut et al., 2007). In contrast to the many studies that use expert-based analysis of LiDAR derivatives to identify landslides, only few studies have attempted to develop computer-aided methods for extracting landslides from single or multiple pulse LiDAR data (McKean and Roering, 2004; Glenn et al., 2006; Bull et al., 2010). All listed studies have been carried out in a pixel-based analysis. However, with high resolution topographical data such as LiDAR, object-oriented analysis (OOA), also referred to as object-based image analysis (OBIA), might provide better results.

OOA has gained increased attention for semi-automated landslide identification from monotemporal (e.g. Barlow et al., 2003, Martha et al., 2010, 2011; Stumpf and Kerle, 2011) and multitemporal (i.e. change detection; Lu et al., 2011) multispectral and panchromatic airborne and satellite imagery. Elevation data have been used before in OOA-based landslide detection work (e.g. Martha et al., 2010, 2011), but only to support the knowledge based removal of false positives and the discrimination of different landslide types.

The identification of old vegetated landslides, not detectable from passive optical imagery, has not been investigated so far. LiDAR derivatives in an OOA have been used for semi-automated geomorphological mapping (van Asselen and Seymonsbergen, 2006; Anders et al., 2011; Drăguţ and Eisank, 2012). In these studies the identification of individual landslides was beyond the scope of the analysis. The objective of this study is to test OOA for landslide inventory mapping using single pulse LiDAR data for both the segmentation and classification steps, without the support of any spectral information. We exploit the profound morphologic manifestation of old, densely vegetated landslides to semi-automatically map their extent using only LiDAR derivatives, and test the analysis in the Flemish Ardennes (Belgium), a hilly region with a rolling topography, affected by more than 200 landslides (Van Den Eeckhaut et al., 2007) and characterised by loose Tertiary deposits with croplands on the plateaus and forests and pastures on the hillslopes and in the valleys. OOA of LiDAR derivatives for landslide extraction contains several interesting challenges. In this study we focus on (1) cognitive perception of landslides as geomorphic features, consisting of parts with significantly different morphometric characteristics, (2) testing scale optimization methods developed for passive optical imagery, and (3) selection of morphometric indicators

* Corresponding author.

for the identification of different landslide features. We further discuss the possibilities and limitations of LiDAR-based segmentation and classification of landslides covered by vegetation.

2. MATERIAL AND METHODS

2.1 Conceptualisation of landslides

The ultimate benchmark of OOA is the translation of cognitive perception (Lang, 2008) into rule sets. Semi-automated classification of landslides represents an attempt to replicate subjective landslide recognition (e.g. Martha et al., 2010; Stumpf and Kerle, 2011). Figure 1 contains the conceptualization of a typical landslide located in its characteristic physical environment in the study area (Flemish Ardennes, Belgium).

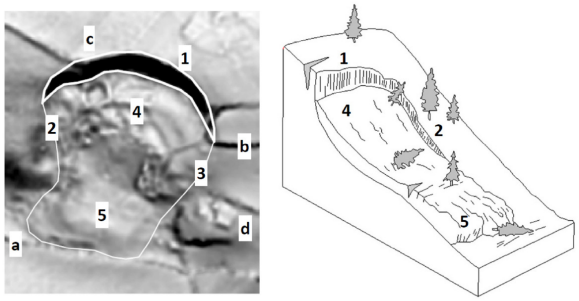

Landslide features	Properties
1. Main scarp	Steep, semi-circular, concave in planform, main direction is perpendicular to flow direction, length/with > 1.
2. Distinct flank	Upslope part has higher elevation than affected area, downslope part is less clear, main direction is perpendicular to main direction of scarp.
3. Indistinct flank	Same as 2, but less clear due to human interventions or soil erosion.
4. Depletion area	Lower than surrounding area due to removal of debris.
5. Accumulation area	Higher than surrounding area due to accumulation of debris.
Other features (inc. false positives)	**Properties**
a. River	Can border landslide foot.
b. Earth bank (field, road)	Steep, length/with > 1.
c. Crop field	Low slope gradient, low roughness, compact shape.
d. Anthropogenic feature (building, quarry)	High roughness, variable dimension, variable topographic location.

Figure 1 Conceptualization of a typical landslide in the soil covered and hilly study area in Belgium. Landslide features (1-5) are defined according to Cruden and Varnes (1996)

A landslide contains several features with significantly different morphologic signatures (Figure 1). The main scarp (1) tends to be the easiest feature to recognize. It is semi-circular (long and narrow) with a steep slope and convex planform, and its polygon has a main direction perpendicular to the flow direction. The fresher the landslide, the more clear also the flanks (2, 3) will be. Landslide flanks form the border between the depletion area where debris has been removed (4) and the original topography, hence they can be distinguished by a distinct change in elevation. As displaced material moves downslope, flanks are most often more or less perpendicular to the main scarp. The displaced material in the depletion and accumulation (5) areas is characterized by a high surface roughness.

Having observed different landslide parts, cognitive visual analysis readily allows them to be conceptually merged into one landslide, even if not all features are clearly present, because they are for example altered by human activities (e.g. buildings, roads). The human brain is further able to distinguish possible false positives (Figure 1), such as earth banks along roads, crop fields (b) and rivers or anthropogenically disrupted terrain (d), which can be similar to main scarps and displaced terrain, respectively.

In OOA, the ultimate objective now is to find a classification rule set using this geomorphic fingerprint of the landslide parts. In this study, the segmentation and classification procedures were calibrated with small samples selected in a 10 km^2 test area in the Flemish Ardennes (see section 3.1; Figure 2). They were then applied to the 50 km^2 area surrounding the test area. For the test and validation area, the existing landslide inventory map obtained through visual inspection of LiDAR derivative maps and field surveys (Van Den Eeckhaut et al., 2007) contains 10 and 28 deep-seated slides, and 4 and 6 possible slides (less clear geomorphic manifestation), respectively. Small, shallow landslides are not taken into account in this study.

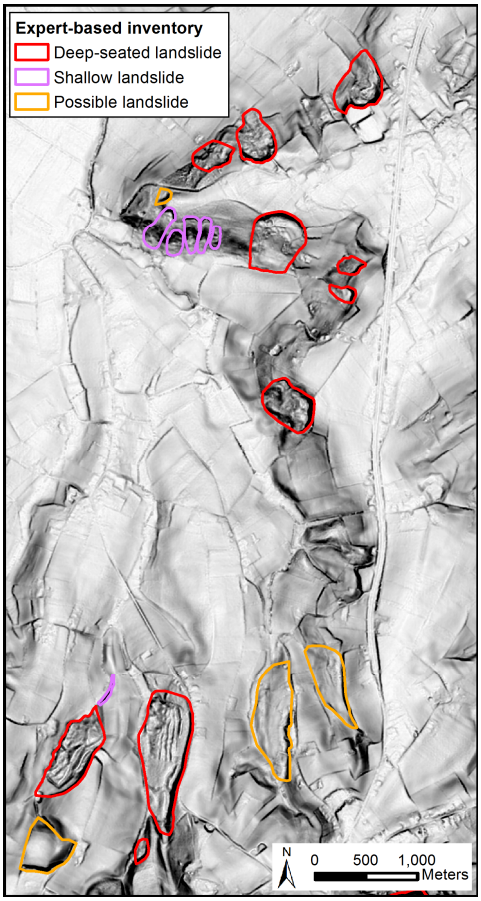

Figure 2 Excerpt of the 10 km^2 test area in the Flemish Ardennes showing the landslide inventory produced by experts (Van Den Eeckhaut et al., 2007) overlaying the diffuse analytical shaded relief map (©AGIV, 2005)

2.2 LiDAR data and derivatives

The LiDAR data of the Flemish Ardennes were collected in 2001 and 2002 (AGIV, 2005). An Azimuth Aeroscan small footprint (30 cm) multi-return LiDAR system with a pulse rate of 15 kHz and vertical accuracy (RMSE) of 4 cm was used. Laser pulses were sent at equal intervals within 600 m wide swaths with average pulse density of 1 per 4 m². Terrascan software was used by the vendor for the production of the bare earth DTM, and a manual check followed. The data have a point density of at least 1 per 20 m², a horizontal accuracy below 15 cm and an average vertical accuracy that depends on vegetation height, decreasing from 7 cm for freshly cut lawn to 20 cm for pastures and forests (GIS-Vlaanderen, 2003). From the LiDAR point data, available in .txt format, a Triangulated Irregular Network (TIN) was derived which was then converted to a Digital Terrain Model (DTM) with a 2 m resolution. This is the advised cell size when using the relation between resolution and distance between the sampled points, and follows the Nyquist frequency concept that the resolution should be at most half the average spacing between the closest point pairs (see Hengl, 2006), which is 4 to 5 m for the available LiDAR data. The LiDAR derivatives evaluated in this study are listed in Table 1.

2.3 Translation of landslide concept to OOA

For translation of the landslide concept in eCognition™, the most distinct landslide characteristics, the 'main scarps', were extracted first, followed by the 'landslide affected area or landslide body' and the 'flanks'. Thresholding or image binarization (Otsu, 1979; i.e. contrast split segmentation in eCognition™) of the slope map provided segmentation level 1 and was carried out to separate 'steep' from 'unclassified' terrain. The 'unclassified' terrain was subsequently split with multiresolution segmentation of the slope, roughness and openness maps, and the thematic layer with the rivers (Table 1). Although the scale factor, a unitless criterion controlling the maximum allowed heterogeneity in a segment with a lower scale factor yielding a higher number of segments, has an important influence on the segmentation results, it might be expected that optimal scale factors will be less clear when using LiDAR derivatives instead of passive optical images for landslide identification, because landslides consist of features with different dimensions and signatures. To find optimal scale factors, we used the Plateau Objective Function (POF; Martha et al., 2011) and compared the optimal scales with those obtained with the Estimation of Scale Parameter tool (ESP; Drăguţ et al., 2010). Analysis of the POF and ESP of the slope, roughness and openness maps showed that for all three maps scale factors of 33-35 (segmentation level 2) and 13 (segmentation level 3) were optimal for segmentation.

For the classification of the segments we adopted support vector machines (SVM), a supervised learning approach for two-group classification problems (Cortes and Vapnic, 1995), increasingly used in conjunction with OOA (Blaschke, 2010). In the segmentation layer selected as most appropriate for a certain object class we sampled up to 12 objects for each class in the 10 km² test area. These were used to train the models, while the other objects were considered testing samples. More specifically, we selected samples of:

(a) 'main scarps' and 'earth banks' (i.e. possible false main scarps) from the 'steep' segments of segmentation level 1 (obtained from the thresholding);

(b) 'large crop fields' with a low surface roughness from segmentation level 2 (multiresolution segmentation with scale factor 35); and

(c) 'landslide body (sub)segments' and 'small segments not affected by landslides' from segmentation level 3 (multiresolution segmentation with scale factor 13).

Object features included in the SVM were mean segment values (slope, plan curvature, openness and roughness), standard deviation of segment values (slope and plan curvature), and segment width. The latter was only used for classification of the 'main scarps' and 'earth banks'. We refer to Van Den Eeckhaut et al. (subm.) for more detailed information.

Image layer (2 m resolution)	**Description *(software tool)***
DTM (m)	*(ArcGIS™)*
Slope gradient (%)	*(Spatial analyst toolbox in ArcGIS™)*
Plan curvature ()	*(Spatial analyst toolbox in ArcGIS™)*
Roughness (m)	Square root of the average squared difference in elevation values from a centre cell and the eight neighbor cells (Riley et al., 1999) *(ILWIS™)*
Sky-view factor [0 – 1]	Diffuse analytical shaded relief map, represents for each observation point the part of the visible sky above the point as seen from a two-dimensional representation (e.g. a point on a plateau is brighter (resulting in higher value) than a point at the bottom of a steep valley because a larger part of the sky can be seen from the plateau than from the valley; Zakšek et al., 2011) *(SVM v1.11)*
Openness Dif_DTM_DTM_{ki} (m) with i=15, 25, 50, 75	Difference between original DTM and DTM_{ki} with DTM_{ki}: map where each grid cell represents the mean elevation value of a moving window with kernel size ki with i=15, 25, 50, 75 (best result was obtained with i=50) *(ArcGIS™)*
Multiple flow direction [0 - 2π]	Direction of the steepest downward slope on the eight triangular facets formed in a 3 x 3 grid cell window centred on the grid cell of interest (Tarboton, 1997) (*TauDEM toolbox in ArcGIS™)*
Thematic layer (vector map)	**Description *(software tool)***
River	*(Hydrology toolbox in ArcGIS™)*

Table 1. LiDAR derivatives used in the study. For a description of the layers derived from standard tools in ArcGIS™ we refer to ArcGIS Desktop Help

For the extraction of 'landslide flanks' and the growing of the main scarps in segment level 3 we used features of circular variables, such as main direction and mean flow direction. As each individual main scarp has a specific slope orientation, landslides were treated individually in a loop. First, we selected the largest main scarp segment and created a zone or region around it. This zone was square-shaped with twice the landslide's main scarp length as length and width. Then landslide flanks were drawn from both outer ends of the main

scarp in a direction opposite to the main scarp's main direction. Once both flanks were obtained the linking of the main scarp and its affected area into one landslide started from the main scarp and evolved in a downslope direction by adding landslide body segments enclosed by the main scarp and flanks. When this process was finished the second largest main scarp was selected, and the flank extraction and growing steps were repeated. In this way the loop continued until all main scarps were processed.

3. RESULTS

3.1 OOA-based landslide inventory

For the 10 km^2 calibration area, the inventory map obtained using the procedure described above is shown in Figure 3. Visual comparison with the expert-based inventory (Figure 2) suggests a good agreement between the maps. A more detailed accuracy assessment is carried out in the next section.

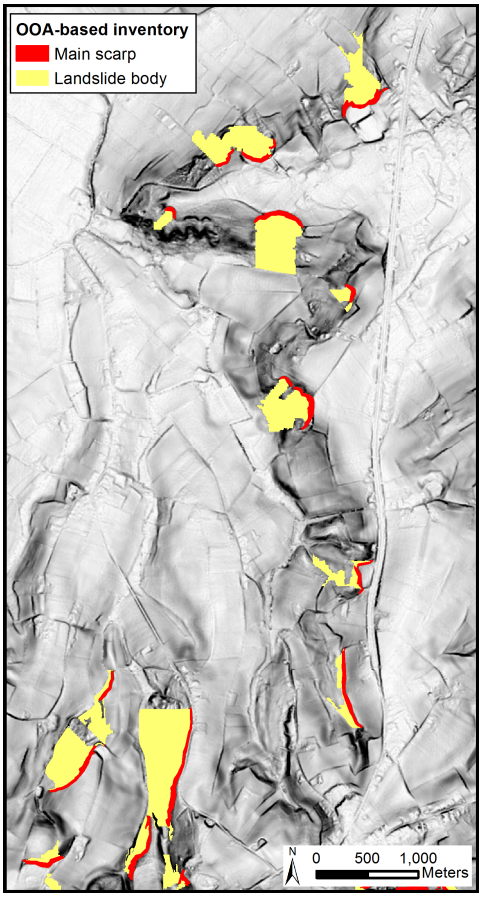

Figure 3 Excerpt of the 10 km^2 test area in the Flemish Ardennes showing the landslide inventory obtained with OOA overlaying the diffuse analytical shaded relief map (©AGIV, 2005)

3.2 Accuracy assessment

Accuracy assessment consisted of a comparison of the landslide inventory obtained with OOA with the expert-based inventory (Figure 2 and 3). No difference in accuracy was found for the test and validation area. This is probably due to the fact that also within the test area only a limited sample of 'main scarps', 'landslide body segments', 'earth banks' and 'crop fields' were used for defining the appropriate morphometric features and their classification rules. The OOA-based inventory contains 90% of the 38 main scarps of clear deep-seated slides. For 71% of the landslides mapped by experts also more than 50% of the landslide body was correctly identified. These results are comparable to the results obtained by Martha et al. (2010) for object-based landslide identification from passive optical imagery in India.

Figure 4 shows two large complex slides (not included in the test area shown in Figure 3) that were not completely identified with OOA. The surface morphology of their affected area is too subdued and affected by anthropogenic interventions, such as construction of houses and roads in the lower deforested part of the landslides.

False negatives or unidentified landslides are landslides for which the main scarp was not correctly identified. In most cases the main scarps were initially identified as scarp candidates though later omitted because of a plan convex morphology.

The OOA landslide inventory contains about 18 false positives, i.e. zones incorrectly classified as main scarps and landslide bodies. These are zones where SVM incorrectly classified either steep valley heads or earth banks as main scarps, and where subsequent growing resulted in delineation of a landslide body. This number of false positives might seem high at first, but this is not really true in our opinion because in the steep valley heads falsely classified as landslides (e.g. rectangle in Figure 4) the occurrence of small, shallow slides might not be excluded.

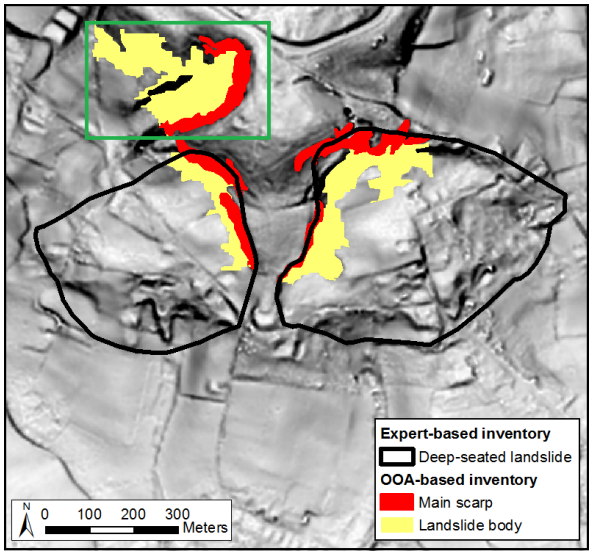

Figure 4: Excerpt of the 50 km^2 validation area showing two landslides identified by experts but only partly identified with OOA, because the surface morphology of the landslides is too subdued and affected by construction of houses and roads. The rectangle shows a valley head incorrectly classified as landslide. The inventory maps are overlaying the diffuse analytical shaded relief map (©AGIV, 2005)

4. DISCUSSION AND CONCLUSIONS

We developed a semantic model for object-based classification of densely vegetated landslides. LiDAR derivatives such as slope gradient, roughness, openness and curvature were tested as an alternative to passive optical images used for identification and mapping of fresh landslides. Using LiDAR derivatives in an OOA we obtained similar accuracy results (i.e. approximately 71%) compared to previous studies using OOA and passive optical remote sensing data (e.g. Martha et al., 2010). A few landslides identified by experts were not identified with OOA because they had a less profound or plan convex main scarp. Some plan concave road banks or river valley heads, on the other hand, were incorrectly classified as landslides.

In soil-covered areas such as Flanders landslides are generally characterized by a much higher surface roughness compared to the surrounding landslide-free areas, and therefore good first results were obtained with slope gradient, surface roughness and openness maps. The downslope parts of old landslides, like those studied here, often have a poor geomorphometric signature. However, this problem has been reported for expert-based landslide inventory mapping to (e.g. Schulz, 2004). In more mountainous areas, however, it is expected to be more difficult to distinguish landslides from non-landslide areas, because stable bedrock outcrops around landslides also have high topographic roughness (Van Den Eeckhaut et al., in press). Additionally, the number of false positive main scarps is higher due to the presence of steep cliffs, and transferability of a rule set calibrated for one or two landslides to other landslides is more problematic.

In OOA, several differences between the use of passive optical remote sensing data and active optical remote sensing data such as LiDAR were observed. The most important one is that when using passive optical remote sensing data, fresh landslides generally consist of one or a few segments only. However, landslides are geomorphologically complex and consist of different parts with different geomorphological characteristics. Hence, they are not represented by one single segment when obtained from LiDAR derivatives and the aggregation from different segments into one final landslide segment is difficult.

This study is the first to analyse different LiDAR derivatives and methods for segmentation of the landslide features. Given the good results obtained so far, it is worthwhile to explore the possibilities of OOA with LiDAR data further. Future research will focus on improving the flank delineation and on more objective selection of LiDAR derivatives to be used for segmentation and classification.

ACKNOWLEDGEMENTS

Part of this study has been carried out in the framework of the EU-FP7 project SafeLand: Living with landslide risk in Europe: Assessment, effects of global change, and risk management strategies (Grant Agreement 226479; http://www.safeland-fp7.eu/).

REFERENCES

AGIV, 2005. LIDAR hoogtepunten – brondata van Digitaal Hoogtemodel Vlaanderen, MVG-LIN-AMINAL-afdeling Water en MVG-LIN-AWZ-afdeling Waterbouwkundig Laboratorium en Hydrologisch onderzoek, Brussels, Belgium, Digital file.

Anders, N.S., Seijmonsbergen, A.C., Bouten, W., 2011. Segmentation optimization and stratified object-based analysis for semi-automated geomorphological mapping. *Remote Sensing of Environment,* 115(12), pp. 2976-2985.

Barlow, J., Martin, Y., Franklin, S.E., 2003. Detecting translational landslide scars using segmentation of Landsat ETM+ and DEM data in the northern Cascade Mountains, British Columbia. *Canadian Journal of Remote Sensing*, 29(4), pp. 510-517.

Blaschke, T., 2010. Object based image analysis for remote sensing. *ISPRS J. Photogramm. Remote Sens.*, 645, pp. 2-16.

Bull, J.M., Miller, H., Gravley, D.M., Costello, D., Hikuroa, D.C.H., Dix, J.K., 2010. Assessing debris flows using LIDAR differencing: 18 May 2005 Matata event, New Zealand. *Geomorphology* 124(1-2), pp. 75-84.

Cortes, C., Vapnik, V., 1995. Support-vector network. *Machine Learning,* 20, pp. 273-297.

Cruden, D.M., Varnes, D.J., 1996. Landslides types and processes. In: Turner, A. K., Schuster, R.L. (eds), *Landslides: Investigation and Mitigation.* Transportation Research Board, National Academy of Sciences, Washington D.C, USA, pp. 36–75.

Drăguţ, L., Tiede, D., Levick, S., 2010. ESP: a tool to estimate scale parameters for multiresolution image segmentation of remotely sensed data. *International Journal of Geographical Information Science*, 24, pp. 859-871.

Drăguţ, L., Eisank, C., 2012. Automated object-based classification of topography from SRTM data. *Geomorphology*, 130(3-4), pp. 21-33.

GIS-Vlaanderen, 2003. Nieuwsbrief GIS-Vlaanderen: Digitaal Hoogtemodel Vlaanderen. Ondersteunend Centrum GIS-Vlaanderen, Gent, Belgium.

Glenn, N.F., Streutker, D.R., Chadwick, D.J., Thackray, G.D., Dorsch, S.J., 2006. Analysis of LiDAR-derived topographic information for characterizing and differentiating landslide morphology and activity. *Geomorphology,* 73(1-2), pp. 131-148.

Hengl, T., 2006. Finding the right pixel size. *Computers and Geosciences*, 32(9), pp. 1283-1298.

Lang, S., 2008. Object-based image analysis for remote sensing applications: modeling reality – dealing with complexity. In: Blaschke, T., Lang, S., Hay, G. (eds), *Object-Based Image Analysis Spatial Concepts for Knowledge-Driven Remote Sensing Applications.* Springer, Berlin, Heidelberg, pp. 3-27.

Lu, P., Stumpf, A., Kerle, N., Casagli N., 2011. Object-oriented change detection for landslide rapid mapping. *IEEE Geoscience and Remote Sensing Letters,* 8(4), pp. 701-705.

Martha, T., Kerle, N., van Westen, C.J., Kumar, K., 2010. Characterising spectral, spatial and morphometric properties of landslides for semi-automatic detection using object-oriented methods. *Geomorphology*, 116(1-2), pp. 24-36.

Martha, T., Kerle, N., van Westen, C.J., Jetten, V., Kumar, K., 2011. Segment Optimisation and data-driven thresholding for knowledge-based landslide detection by object-based image analysis. *IEEE Transactions on Geoscience and Remote Sensing,* 49, pp. 4928-4943.

McKean, J., Roering, J., 2004. Objective landslide detection and surface morphology mapping using high-resolution airborne laser altimetry. *Geomorphology*, 47, pp. 331-351.

Otsu, N., 1979. A Threshold Selection Method from Gray-Level Histograms. *IEEE Transactions on Systems, Man, and Cybernetics*, 9(1), pp. 62-66.

Riley, S.J., DeGloria, S.D., Elliot, R., 1999. A terrain ruggedness index that quantifies topographic heterogeneity. *Intermountain Journal of Sciences*, 5(1-4), pp. 23-27.

Schulz, W.H., 2004. Landslides mapped using LIDAR imagery, Seattle, Washington, U.S. Geological Survey Open-File Report 2004-1396.

Stumpf, A., Kerle, N., 2011. Object-oriented mapping of landslides using Random Forests. *Remote Sensing and Environment*, 115(10), pp. 2564-2577.

Tarboton, D.G., 1997. A New Method for the Determination of Flow Directions and Contributing Areas in Grid Digital Elevation Models. *Water Resources Research*, 33(2), pp. 309-319.

van Asselen, S., Seijmonsbergen, A.C., 2006. Expert-driven semi-automated geomorphological mapping for a mountainous area using a laser DTM. *Geomorphology*, 78, pp. 309-320.

Van Den Eeckhaut, M., Poesen, J., Verstraeten, G., Vanacker, V., Nyssen, J., Moeyersons, J., Van Beek, L.P.H., Vandekerckhove, L., 2007. The use of LIDAR-derived images for mapping old landslides under forest. *Earth Surface Processes and Landforms*, 32, pp. 754-769.

Van Den Eeckhaut, M., Kerle, N., Hervás, J., Poesen, J., Supper, R., in press. Mapping of landslides under dense vegetation cover using object-oriented analysis and LiDAR derivatives. *Proceedings of the 2nd World Landslide Forum*, 3-9 October, 2011, Rome, Italy.

Van Den Eeckhaut, M., Kerle, N., Poesen, J., Hervás, J., subm. Object-oriented identification of forested landslides with derivatives of single pulse LiDAR data. *Geomorphology*.

Zakšek, K., Oštir, K., Kokalj, Z, 2011. Sky-View Factor as a Relief Visualization Technique. *Remote Sensing,* 3, pp. 398-415.